OFFICE OF NAVAL RESEARCH

GRANT: N00014-97-1-0417

PR NUMBER: 97prO-1030

Dr. Richard Carlin

Technical Report #14

Temperature and Field Dependence of Protonated Water Cluster Emission from Field Adsorbed Water Layers on Platinum

by
Christopher J. Rothfuss, Valentin K. Medvedev, and Eric M. Stuve

Submitted to: *Journal of Chemical Physics*

University of Washington
Department of Chemical Engineering
Box 351750
Seattle, WA 98195-1750

July 31, 2001

REPORT DOCUMENTATION PAGE

2. July 31, 2001

3. Interim Report

4. "Temperature and Field Dependence of Protonated Water Cluster Emission from Field Adsorbed Water Layers on Platinum"

5. GRANT: N00014-97-1-0417 , PR Number: 97prO-1030,

6. Christopher J. Rothfuss, Valentin K. Medvedev, and Eric M. Stuve

7. Professor Eric M. Stuve, University of Washington, Department of Chemical Engineering, Box 351750, Seattle, WA 98195-1750

8. TECHNICAL REPORT NO. 14

9. Office of Naval Research,
800 North Quincy Street
Arlington, VA 22217-5660

11. Submitted to: *Journal of Chemical Physics*

12. Reproduction in whole or in part is permitted for any purpose of the United States Government. This document has been approved for public release and sale; its distribution is unlimited.

13. Abstract:

Water ion cluster formation in high electric fields was characterized on a Pt emitter tip over temperatures ranging from 170 to 300 K. Ion clusters emitted from the field-adsorbed water layer were mass resolved using a Wien filter. Two series of tests were conducted to characterize the ion cluster formation. In the first, tip temperature and water pressure were held constant while the applied field at the tip was ramped linearly with time. As the field was increased, water ion clusters $H^+(H_2O)_n$ were emitted, beginning with large n clusters (up to 7) and proceeding through each lower n cluster in turn. The ion emission onset field was found to depend on the value of n and is lower for larger n clusters. The onset of ionization for each cluster was observed to be relatively constant as a function of temperature, however, ion signal intensity was temperature dependent. For the second series of tests, tip temperature was cyclically ramped while the applied field was held constant. The cyclical ramping experiments provided Arrhenius graphs showing thermal deactivation energies for ion emission from the tip. The observed deactivation corresponds to thermal desorption of the n^{th} solvating water molecule of the ion cluster, i.e., the energy associated with the solvation of the proton by the n^{th} solvating water molecule. These energies were found to be 0.85 eV, 0.76 eV, and 0.55 eV for $n = 3$, 4, and 5, respectively.

14. Subject terms: water, field-ionization, protonated water clusters, solvation, electric field

15. No. of pages: 34

17. Unclassified

18. Unclassified

19. Unclassified

20 Unclassified

Temperature and Field Dependence of Protonated Water Cluster Emission from Field Adsorbed Water Layers on Platinum

Christopher J. Rothfuss, Valentin K. Medvedev and Eric M. Stuve

University of Washington
Department of Chemical Engineering
Box 351750
Seattle, WA 98195-1750

Abstract

Water ion cluster formation in high electric fields was characterized on a Pt emitter tip over temperatures ranging from 170 to 300 K. Ion clusters emitted from the field-adsorbed water layer were mass resolved using a Wien filter. Two series of tests were conducted to characterize the ion cluster formation. In the first, tip temperature and water pressure were held constant while the applied field at the tip was ramped linearly with time. As the field was increased, water ion clusters $H^+(H_2O)_n$ were emitted, beginning with large n clusters (up to 7) and proceeding through each lower n cluster in turn. The ion emission onset field was found to depend on the value of n and is lower for larger n clusters. The onset of ionization for each cluster was observed to be relatively constant as a function of temperature, however, ion signal intensity was temperature dependent. For the second series of tests, tip temperature was cyclically ramped while the applied field was held constant. The cyclical ramping experiments provided Arrhenius graphs showing thermal deactivation energies for ion emission from the tip. The observed deactivation corresponds to thermal desorption of the n^{th} solvating water molecule of the ion cluster, i.e. the energy associated with the solvation of the proton by the n^{th} solvating water molecule. These energies were found to be 0.85 eV, 0.76 eV and 0.55 eV for $n = 3$, 4 and 5, respectively.

Introduction

Dissociative ionization of water is fundamental to electrochemistry and is known to be influenced by electric field[1]. Near the surface of an electrode, charge is screened over a short distance resulting in very high fields on the order of 1-3 V/Å[2-4]. This region, the electrochemical double layer, is chemically active due to its high field. While often thought of as a continuous, one dimensional feature, the field is actually quite dynamic and inhomogeneous due to finite size effects of the electrolyte molecules. Experimental studies of protons and hydroxyl groups in high fields near surfaces provide insight into the properties of the electrochemical double layer and help to describe in better detail the behavior of ionic species in high fields. Field emitter tips provide a small controlled arena for analyzing high field chemical reactions, solvation energies, field induced migration and fundamental chemical properties of adsorbed chemical species under ultra-high vacuum (UHV) conditions.

The study of water on a field emitter tip dates back to 1955 when Gomer and Inghram[5] observed the formation of ion clusters on a tungsten tip. Beckey et al.[6] further characterized water ionization by identifying the emitted ions as protonated water clusters of varying size. Schmidt[7] later provided critical ionization potentials for water on tungsten, iridium and platinum. Anway[8] extended field ionization experiments to field adsorbed water layers at room temperature. More recently, Stintz and Panitz have studied both protonated water clusters[9,10] and negative ion water clusters[11] using a technique called ramped field desorption (RFD) and characterized the sizes of the ion clusters produced as the emitter tip field was ramped. Recent work by our group[12-15] has probed the onset of ionization of these water clusters from a Pt emitter tip as a function of the adsorbed layer thickness and tip temperature in an effort to investigate the mechanism of ionization and the response of the nearby, non-reactive water

molecules. Additionally, recent molecular dynamics studies and *ab initio* calculations have attempted to quantify dissociation probabilities for water[16], as well as solvation energies[17,18], solvation dynamics[19], and local electric fields[20] present in liquid water and ice.

For the work described in this paper, water on the platinum tip resides in a field adsorbed layer in equilibrium with a constant background pressure of water in the vacuum chamber. The background pressure is maintained below the condensation point for water at the experimental temperature. The emitter tip conditions used in this work provide an environment for investigating ion cluster formation from a liquid-like water layer with control over applied field, tip temperature, and water flux under steady state conditions. Field desorbed ions were mass resolved using a Wien filter and monitored in real time without perturbing the system. Mass resolved, ramped field ionization was performed over a range of temperatures from 170 to 300 K. This provided insight into the field dependence of ion cluster emission. Additionally, temperature cycling experiments were performed at constant fields to examine proton solvation energies of small clusters.

Experimental Apparatus

The experimental setup, which has been described previously[15], consisted of an ultra-high vacuum (UHV) chamber pumped by a turbomolecular and titanium sublimation pumps to a base pressure of 10^{-10} Torr. A Pt tip of approximately 350 Å radius and {100} orientation was spot-welded to a 0.25 mm Pt wire heating loop and mounted onto a liquid nitrogen cooled downtube. The cryo-cooled tip, at a base temperature of 105 K, was resistively heated to the desired experimental temperature. Tip temperature was measured with a chromel-alumel thermocouple spot-welded to the heating loop near the tip. The tip potential was controlled with a ± 5 kV

power supply. A planar counter electrode with a 5 mm circular hole was positioned coaxial with the tip apex at a distance of 1 mm. The counter electrode potential was independently regulated to ± 5 kV. The tip/counter electrode configuration provided fields greater than 4 V/Å, sufficient to field-evaporate Pt and thus clean the tip. The downtube with tip assembly was mounted onto a polar coordinate manipulator for orientation towards either a microchannel plate/phosphor screen assembly for ion/electron imaging, or a Wien filter assembly for mass resolved analysis of emitted ions. Water vapor was introduced into the chamber through a variable leak valve. The water sample used for dosing was prepared by triply freezing nanopure, de-ionized water to 77 K and evacuating the containment vessel. A final freeze and evacuation of the vessel was performed at 195 K.

The Wien filter assembly, shown in Figure 1, consisted of an entrance diaphragm (b_1), focusing lens (b_2-b_4), Wien filter (c), bellows (d) for changing the distance between the tip assembly and the focusing lens, drift tube (e), and a pair of chevron multi-channel plates (MCPs) with a phosphor screen (f) for detecting and imaging the exiting ion beam. The focusing lens was similar to the symmetric three-electrode unipotential type suggested by Rempfer [21]. To eliminate aberrant electrical fields, stainless steel cylindrical rings were welded to the entrance and end electrodes of the lens in its inner part. The addition of these rings to the usual design of the unipolar lens improved focusing of the ion beam. The lens was mounted on four supporting stainless steel rods that passed through the Wien filter, allowing the distance between the tip and the entrance diaphragm connected to the lens to be varied between 20 and 56 mm. With a 5 mm diameter hole in the entrance diaphragm, ions emitted from the tip within the space angle of 0.109 (at 20 mm) to 0.014 steradians (at 56 mm) were collected by the Wien filter assembly. For a typical tip, ions are emitted from the tip surface through angles up to ~60° from the tip axis,

based on comparisons of field ion micrographs to stereographic maps of the crystalline structure. Field compression of the ion beam effectively reduces this angle to ~40°. The space angle of the total emission cone from the tip is 2π [1-cos(θ)] ≅ 1.5 steradians, i.e. our Wien filter can analyze from 1% to 7% of the ions emitted from the tip depending on the position of the entrance diaphragm. For experiments with tips of radius 350 Å, ion signals of 10^3 counts/s were easily achieved at the exit of the Wien filter, which would then imply total ion emission of $10^4 - 10^5$ s^{-1}.

The Wien filter itself was constructed with curved magnetic and electric poles[22] providing homogeneity of electric and magnetic fields in the functional space of the filter. The length of the magnetic poles along the cylindrical axis was 100 mm. The electrodes were longer than the magnetic poles by 1.3 mm on each side to decrease aberrations in the boundary regions at the entrance and exit of the Wien filter.

A beam of ions with mass m_0 and energy $e\phi_0$, where ϕ_0 is the accelerating potential for an ion (i.e., potential of the tip in reference to ground) and e is the ion charge, follows a straight path through the crossed electrical and magnetic fields of a Wien filter when the electrical force, eF, is equal to the magnetic force evB, where F is the field strength, v is the ion velocity perpendicular to the magnetic field, and B is the magnetic field strength, giving

$$F = B\sqrt{\frac{2e\phi_0}{m_0}}. \qquad (1)$$

For ions of differing masses in the same accelerating potential, the electrical and magnetic forces will not be balanced. As a result, each ion is shifted to the left or right in the plane of the electric field, depending on whether its mass m is greater or less than m_0. If the length of the Wien filter is L (100 mm in our case) and the distance between the Wien filter and the

microchannel plate is L_1, then the shift in the position of the spot created by a beam of mass m in the MCP plane is

$$\Delta x = \frac{F}{2\phi_0}\left(\frac{L^2}{2} + LL_1\right)\left(1 - \sqrt{\frac{m_0}{m}}\right). \quad (2)$$

For our system, the drift tube between the bellows and the multichannel plate was 616 mm in length, giving a total L_1 of about 800 mm depending on the bellows length. With a distance between the two Wien filter electrodes of 12.9 mm for our system,

$$\Delta x / \text{mm} = 3.3 \cdot 10^3 \frac{\Delta V}{\phi_0}\left(1 - \sqrt{\frac{m_0}{m}}\right), \quad (3)$$

where ΔV is the potential difference between the electrode pair (c_3). We used this equation to calculate the minimum electrode potential needed to completely separate two neighboring masses so that only one ion signal was registered on the MCPs. For our MCPs (19 mm diameter) with ϕ_0 at 3000 V, ions of mass 18 (H_2O^+) and mass 19 (H_3O^+) were separated at an electrode potential of 550 V, while all other ion beams examined herein (other protonated water clusters with m up to 127) were separated with 150 V.

Direct imaging of the mass selected ion beam using a CCD camera positioned behind the phosphor screen and MCP assembly was of considerable value for tuning the ion signal. The imaging ensured good ion focus and allowed us to confirm that no signal from neighboring masses was registered on the MCPs.

Experimental Procedure

Two series of tests were conducted to characterize water ion cluster formation in a field-adsorbed water layer on the platinum emitter tip. In the first, the Wien filter was used for mass

selecting a particular water cluster ion signal for a series of isothermal ramped field ionization and desorption experiments. For the second, the tip potential was held constant at the ion signal maximum while the temperature was cycled for each of a series of selected masses.

Prior to all testing, the Pt emitter tip was field cleaned and imaged with neon gas. Cleaning was accomplished by field evaporating a small amount of Pt from the surface, while visually inspecting the imaged surface until it appeared atomically clean and structured. Simple annealing of the tip is not sufficient for removing all contaminants from the surfaces - particularly carbon. Field cleaning ensures complete removal of surface contaminants prior to testing and reduces the possibility of undesired surface reactions or interactions. During field cleaning, several layers of Pt were field evaporated and the tip crystalline structure was visually inspected to guarantee pristine tip conditions. During imaging, the best imaging voltage (BIV) was recorded and used to estimate the tip radius with the formula

$$F_{app} = \frac{V_t}{\beta r_t} \tag{4}$$

where F_{app} is the applied field, V_t the tip potential, r_t the tip radius and β is a shape factor commonly taken as equal to 5 for our tip geometry [23]. At the best imaging potential in neon, the field is known to be 3.75 V/Å [24]. Throughout this paper, field is reported as the applied field, which is the field that would be present at the tip surface for the applied voltage V_t in the absence of any adsorbate.

Mass Selected Ramped Field Ionization and Desorption

After imaging and field cleaning, the tip potential V_t and counter electrode potential V_{CE} were set to +3 kV. To maintain a constant ion formation potential with respect to ground, the tip potential was held constant while the counter electrode potential was ramped negatively to

increase the local field. The constant ion formation potential corresponds to constant ϕ_0 in Eq. 1 and is important for both lens focusing and consistent Wien filter results. The cryo-cooled tip was then resistively heated to the desired experimental temperature, ranging from 180 to 300 K. This temperature range is above the field free condensation temperature for water on platinum, typically 165 K depending on pressure. Water was then introduced into the chamber at a pressure of $5 \cdot 10^{-6}$ Torr. The Wien filter was tuned to select a particular ion mass. The counter electrode potential was ramped from +3000 V to 0 V at a rate of 10 V/s. A computer data acquisition system recorded the mass selected ion signal as a function of potential. The Wien filter was then tuned to a different mass, and the ramping procedure was repeated. Three or more experiments for each tested mass were performed in 10 K increments from 180 to 300 K.

Mass Selected Field Ionization and Desorption with Temperature Cycling

These experiments were performed in a fashion similar to the ramped field experiments described above with a few notable exceptions. The counter electrode potential for each experiment was set to the potential that provided the optimal ion signal for the desired water cluster. The Wien filter was again tuned to isolate the ion signal for the selected mass. Prior to introducing water at a partial pressure of $5 \cdot 10^{-6}$ Torr, the tip was heated to 300 K. This temperature prohibited formation of water ion clusters with n greater than 2. The temperature, regulated with a computer controller card, was then ramped down to 170 K and slowly cycled between 170 K and a temperature above the maximum cluster formation temperature for the selected mass: 300 K for $H^+(H_2O)_3$, 260 K for $H^+(H_2O)_4$, and 240 K for $H^+(H_2O)_5$. Each full cycle lasted 10 minutes. Typically, 5 cycles were run consecutively for a given mass, after which the tip was heated above 300 K and briefly field cleaned at 3 kV before beginning the next

series of cycles. The ion signal was sampled twice per second by the computer and recorded along with the time and tip temperature.

Results

The mass selected ramped field ionization and desorption experiments revealed ion cluster formation dependencies on both tip temperature and applied field as expected. Figure 2 depicts the ion signals for detected water clusters at 180 K and 230 K as a function of applied field. The graph represents signal averaged data for three or more runs per mass. At low temperatures, $H^+(H_2O)_n$ ion clusters were detected for n up to 7. The large n ion clusters were favored at lower field strengths. As the field increases, each ion cluster gives way to the next lower cluster number until the onset of direct ionization of H_2O to form H_2O^+. At higher temperatures, the same progression through the ion clusters occurs, though large ion cluster signals are diminished or absent entirely. Although the amplitude of the ion signal for a given mass varies significantly with temperature, the field dependence of the cluster formation does not. These results allowed us to determine field and temperature conditions that strongly favored the formation of particular ion cluster types.

Figure 3 illustrates typical experimental temperature dependencies of the ion signals for masses 55, 73, and 91 at their respective optimal signal potentials as determined from Figure 2. The initial temperature was chosen above the range where ion formation was observed. As the temperature decreases linearly with time, the ion signal increases for each mass. After reaching a minimum temperature, chosen to remain above the field free condensation point, the temperature was increased, resulting in a decrease in ion signal, as expected. No hysteresis effects were observed in our experiments.

The ion signal versus inverse temperature was plotted using data from approximately 15 cycles for each of the three masses. This provides an Arrhenius type plot, shown in Figure 4, which can be used to determine activation energies for each of the cluster formation events. The apparent activation energies for ion clusters $n = 3$, 4, and 5 were 0.85 ± 0.03, 0.76 ± 0.02, and 0.55 ± 0.02 eV, respectively. Higher mass clusters ($n > 5$) were not present over a wide enough temperature range to extract activation energies. Lower mass clusters ($n < 3$) were present over the entire experimental range and were therefore not suited for the same Arrhenius analysis.

Discussion

Ion Cluster Emission

The results of the mass selected ramped field ionization experiments in Figure 2 show that the field necessary for emitting ion clusters varies with ion cluster size. Large ion clusters are more easily emitted than small clusters and were consequently observed at much lower fields. The field required for emission of a specific ion did not vary significantly between the two temperatures, although the ion current for the higher masses diminished at higher temperatures. The ease of cluster emission depends on the difference in energy between the solvated proton in the water layer on the surface and the proton solvated by n water molecules in vacuum near the surface. Figure 5 qualitatively illustrates the behavior of the energy barriers at 0.3 and 0.9 V/Å for cluster emission in the presence of a strong field. The field free energies necessary for removing a given ion cluster were calculated with a thermodynamic cycle. For example, a proton near the water surface may be created by first removing a water molecule from the bulk by providing the latent heat of vaporization λ_v of 0.44 eV [25],

$$ {}^{\ell}H_2O \rightarrow {}^{v}H_2O \tag{5} $$

dissociating it in vacuum with a dissociation energy E_D of 5.11 eV [26],

$$ {}^{v}H_2O \rightarrow {}^{v}H + {}^{v}OH \tag{6} $$

ionizing the hydrogen with an ionization potential I_P of 13.6 eV [25],

$$ {}^{v}H + {}^{v}OH \rightarrow {}^{v}H^{+} + {}^{v}OH + e^{-} \tag{7} $$

transferring the free electron to the OH with an electron affinity E_A of -1.83 eV (here given as negative for consistency) [25],

$$ {}^{v}H^{+} + {}^{v}OH + e^{-} \rightarrow {}^{v}H^{+} + {}^{v}OH^{-} \tag{8} $$

and then solvating the hydroxide ion with a solvation energy of $E_{solv}^{OH^-}$ of -4.77 eV [27].

$$ {}^{v}H^{+} + {}^{v}OH^{-} \rightarrow {}^{v}H^{+} + {}^{\ell}OH^{-} \tag{9} $$

Summing the energies

$$ \Delta E_{emit}^{H+} = \lambda_v + E_D + I_P + E_A + E_{solv}^{OH-} \tag{10} $$

results in a total energy ΔE_{emit}^{H+} of 12.55 eV for the emission of a proton from bulk water. Solvating the proton,

$$ {}^{v}H^{+} \rightarrow {}^{\ell}H^{+} \tag{11} $$

results in an initial energy of 0.7 eV[14]. This initial state assumes infinite solvation ($n \rightarrow \infty$), which may not be the case on the Pt surface, although the Pt surface itself may act to solvate the proton to some extent. Energies for ion clusters of different n may then be calculated by accounting for the additional energy of solvation [28] of the emitted proton by the n water molecules, minus the energy required to remove the water molecules from the bulk according to,

$$ \Delta E_{emit}^{n} = \Delta E_{emit}^{n-1} + \Delta E_{solv}^{n} + \lambda_v \tag{12} $$

where ΔE_{emit}^{n} is the energy barrier for cluster n emission and ΔE_{solv}^{n} is the solvation energy due to

the n^{th} solvating water molecule. The values for the first several ion clusters are tabulated in Table 1.

As Figure 5 demonstrates, the energy barrier for ion emission is formed by a combination of the image potential and the field lines. The image potential V_I is described by,

$$V_I = \frac{e^2}{4x}\left(\frac{\varepsilon - 1}{\varepsilon + 1}\right) \tag{13}$$

where ε is the relative permittivity and x the distance from the surface [29]. This expression is for a point charge approaching a perfectly smooth flat surface, and is therefore only an approximation for the emitter tip. It is nonetheless reasonable when comparing the thickness of <10 Å for thin water layers to the tip diameter ~350 Å. Additionally, the image force expression has a singularity at the water-vacuum interface and consequently fails within the first Ångstrom, but this is acceptable for a qualitative consideration of the energy barrier peak, which occurs beyond the first Ångstrom. The field is approximately linear near the water vacuum interface for a thin water layer [30] and is shown as such. The energy barriers under field free conditions for clusters n = 1-4 are depicted by dashed lines at the top of each diagram. A solid line shows the emission barrier E_b due to the combined field and image forces (neglecting higher order terms) for each cluster given by,

$$E_b(x) \cong \Delta E_{emit} - xF - V_I(x). \tag{14}$$

As shown, the energy barriers are confronted by a solvated proton at 0.7 eV in the water layer on the tip. This initial energy is the same as the thermal barrier for H_2O ionization discussed earlier. At low fields the barriers are high and wide. As the field increases, the barrier narrows and decreases. Thermally activated emission may occur depending on the barrier height. When the emission barrier for a given cluster falls below the potential energy of the solvated proton,

emission occurs freely. As the field increases further, the emission barriers for each cluster n in turn drop below the solvated proton potential and become energetically accessible.

It is important to note that the applied field shown in Figure 5 is idealized. The local field at the ion cluster emission point may be enhanced due to the formation of localized humps[31] on the surface where the water supply function appears to be concentrated. In addition to the influence of localization on the energetics of emission, localization plays a role in the kinetics of the cluster formation. While large n cluster emission is energetically favorable, kinetically it is more difficult to achieve because it requires further solvation. Consequently, the lowest n cluster that is energetically accessible at a given field and temperature will dominate the ion emission signal. This is observed in the results of the ramped field ionization experiments shown in Figure 2. When cluster n emission is observed to decay during the field ramp, cluster n-1 emission begins. Cluster n emission is still energetically favorable, but the cluster is capable of overcoming the emission barrier after reaching n-1. For example, the peak of cluster 3 emission occurs at an applied field of 0.43 V/Å, the same field as the onset of emission for cluster 2. As cluster 2 emission increases, cluster 3 emission decays, even though cluster 3 emission is still energetically favorable.

Temperature Dependence and Solvation Energy

A comparison of the ion emission signal heights of the 180 K and 230 K ramped field ionization experiments for large n clusters shows a dependence of signal intensity on tip temperature. At higher temperatures the large n cluster emission was diminished, even though the required emission fields were equal. By maintaining the tip at a constant field selected to optimize a chosen cluster and cyclically ramping the temperature, the temperature dependence of

the emission amplitude was observed, as illustrated by Figures 3 and 4. An added benefit of these constant field experiments is that the water supply to the tip is relatively constant, as opposed to the ramped field ionization experiments where the flux of water to the tip is influenced by the applied field.

From the Arrhenius plots in Figure 4, several observations may be made about the behavior of the ion clusters. While the signal for the $n = 5$ cluster diminishes with increasing temperature, the $n = 4$ signal remains saturated. As the $n = 5$ fades away completely, the $n = 4$ signal begins to decay, although the $n = 3$ remains saturated. Finally, when the $n = 4$ emission ceases, the $n = 3$ signal decays. That is, there is continuity in the progression of the decay with temperature of the ion signals from one cluster to the next. The decrease in emission signal with increased temperature is in contrast to traditional Arrhenius plots depicting temperature activated reactions. For these data, ion emission appears to be a thermally *deactivated* event. This suggests an alternate pathway to field ionization that depends strongly on temperature and consequently shuts down the emission event as the thermally activated alternate pathway begins to dominate.

There are three primary reactions governing the ion formation and emission processes. These reactions are illustrated in Figure 6a. The first of these reactions,

$$H_2O^* \xleftrightarrow{r_a} H_2O \tag{15}$$

governs the supply of water to the surface, where H_2O^* is gas phase water and H_2O is surface adsorbed water and not part of an ion solvation shell. Reactants discussed hereafter are surface adsorbed unless denoted by an asterisk to indicate gas phase. The net reaction rate r_a may be expressed as

$$r_a = k_1 p_w - k_2 \theta_w \tag{16}$$

where k_1 and k_2 are reaction rate constants, p_w the water partial pressure, and θ_w the surface water coverage for sub-monolayer quantities only. For multilayers cases θ_w will be constant. This equation may be equivalently restated as

$$r_a = NS - k_2\theta_w \tag{17}$$

where N is the incident water flux and S is the sticking coefficient. The remaining rate constant is given by

$$k_2 = A_2 e^{-\lambda_v/kT} \tag{18}$$

where A_2 is a pre-exponential factor. Although λ_v for water on platinum is not exactly equal to the value for bulk water, the difference is not significant for these calculations.

If we consider the case where a variety of clusters has already formed on the surface, the second reaction equation,

$$H^+(H_2O)_{n-1} + H_2O \xleftrightarrow{r_b^{(n)}} H^+(H_2O)_n \tag{19}$$

accounts for the solvation of the protonated water molecule with the transition of the solvation shell from n-1 to n and is depicted specifically in Figure 6b. The net rate of this reaction,

$$r_b^{(n)} = k_3^{(n)}\theta_{n-1}\theta_w - k_4^{(n)}\theta_n \tag{20}$$

and the corresponding rate constants, k_3 and k_4, vary with n and are superscripted accordingly. θ_n represents the surface coverage by n solvated proton clusters, i.e. $H^+(H_2O)_n$. θ_w once again assumes sub-monolayer coverages. The forward reaction constant, given by

$$k_3^{(n)} = A_3^{(n)} e^{-E_A^{(n)}/kT} \tag{21}$$

has a low activation barrier $E_A^{(n)}$ as water readily solvates the proton under experimental conditions and should proceed rapidly. The forward reaction is exothermic and will release the excess energy of solvation $\lambda_E^{(n)}$ which is the difference in energy between the water molecule as

the n^{th} member of the solvation shell, and the water molecule on the surface with no role in solvation. The rate constant for the desolvation reaction, stepping from n to n-1, is given by

$$k_4^{(n)} = A_4^n e^{-(E_A^{(n)} + \lambda_2^{(n)})/kT} \tag{22}$$

The energy barrier for the reverse reaction is higher than that of the forward reaction by the value of the excess energy of solvation.

The third reaction of interest is the ion emission event,

$$H^+(H_2O)_n \xrightarrow{r_c^{(n,m)}} H^+(H_2O)_{m\le n}^* + (n-m)H_2O \tag{23}$$

where a cluster of size $m \le n$ is emitted from a cluster of size n on the surface, leaving behind n-m surface adsorbed water molecules. This reaction is, for all practical purposes, irreversible in the presence of a strong applied field, and may therefore be given by

$$r_c^{(n,m)} = k_5^{(n,m)}\theta_n \tag{24}$$

where the doubly superscripted reaction rates and constants depend on both the initial surface cluster size and the size of the emitted ion cluster. The reaction constant may be written as

$$k_5^{(n,m)} = A_5^{(n,m)} \exp\left(\frac{-E_{Emit}^{(n,m)}(F)}{kT}\right) \tag{25}$$

where the activation barrier $E_{Emit}^{(n,m)}$ is a strongly field dependent value as suggested by Figures 2 and 5. $E_{Emit}^{(n,m)}$ is equivalent to E_b mentioned earlier while discussing emission barriers, but accounts for the incomplete solvation of the surface ion with the double superscript.

Four additional reaction equations are necessary for completion. The first is the dissociative ion formation event,

$$H_2O \xrightarrow{r_d} H^+ + OH^-. \tag{26}$$

This reaction is temperature and field dependent. The rate may be estimated for our

experimental conditions using methods outlined by Pinkerton et al. [15]. For tested experimental conditions, this dissociation reaction is much greater than the ion emission rate and is not rate limiting.

The second equation is the electron discharge at the tip surface,

$$OH^- \xrightarrow{r_e} OH + e^-_{Pt}. \tag{27}$$

Conservation of charge at equilibrium dictates that the reaction rate of Equation 27 will be equal to the total ion emission rate. Accounting for the buildup of OH on the surface provides, in a non-elementary reaction,

$$2OH \xrightarrow{r_f} H_2O + O \tag{28}$$

The fate of the atomic oxygen on the surface is not known for certain. It may diffuse up the tip shank, recombine with neutralized hydrogen (if available) or, at high fields, ionize and desorb from the Pt tip according to the reaction,

$$2O \xrightarrow{r_g} O_2^{+*} + e^-_{Pt} \tag{29}$$

as suggested by Ernst, et al. [32]. The exact mechanism, however, does not prove important to the steady state calculation.

The rate of change of water on the tip surface may be expressed using the rate equations given above. This results in the differential equation

$$\frac{d\theta_w}{dt} = r_a - \sum_0^{\infty} r_b^{(i)} + \sum_{i=1}^{\infty}\sum_{j=1}^{i}(i-j)r_c^{(i,j)} - r_d + r_f \tag{30}$$

where the first term on the right hand side of the equation accounts for the adsorption/desorption flux, the second for the summation of the solvation reactions, the third for the water left behind by all of the emission events, and the final two terms due to the dissociative ionization and OH recombination events, respectively. By varying the temperature very slowly and maintaining

constant tip potential during testing, the tip surface may be assumed to be at steady state. This allows us to set the time derivative to zero. Additionally, it allows us to set serial pathways at equal rates (while accounting for stoichiometric multipliers). By setting the tip to conditions where emission of only one cluster type dominates and occurs readily, ion emission will be restricted to the case where $n = i = j$, thereby eliminating the third term from the equation. The water dissociation rate r_d is not rate limiting and is therefore taken at equilibrium and may be set equal to $r_b^{(n)}$. The OH recombination reaction also must be at equilibrium resulting in r_f equal to $^1/_2\ r_b^{(n)}$. Since emission will not proceed until the n^{th} solvation is reached, n solvation events must occur per emission event. When we take these as serial events and take into consideration the fact that the ion emission event is a one-to-one function of the rate of formation of n size clusters at steady state we may simplify the equation and are left with

$$r_a - \left(n + \tfrac{1}{2}\right) r_b^{(n)} = 0 . \tag{31}$$

Plugging in the equations for the rate constants and solving for the surface coverage of water, θ_w, gives

$$\theta_w = \frac{NS + (n + \tfrac{1}{2})\theta_n k_4^{(n)}}{k_2 + (n + \tfrac{1}{2})\theta_{n-1} k_3^{(n)}} . \tag{32}$$

Next, we turn to the rate of change of the surface population of n solvated protons, which is described by the differential equation

$$\frac{d\theta_n}{dt} = r_b^{(n)} - r_b^{(n+1)} - \sum_{i=0}^{n} r_c^{(n,i)} . \tag{33}$$

Again, we take the system at conditions optimal for forming ion clusters of size n only. Since emission of cluster n+1 is more easily accomplished than emission of cluster n, failure to emit size n+1 clusters allows us to assume $r_b^{(n+1)} << r_b^{(n)}$ and that the summation term is

approximately $r_c^{(n,n)}$ (hereafter referred to as $r_c^{(n)}$). This reduces the equation to

$$\frac{d\theta_n}{dt} \cong r_b^{(n)} - r_c^{(n)}. \tag{34}$$

With the tip at steady state conditions we further reduce this to

$$r_b^{(n)} - r_c^{(n)} = 0. \tag{35}$$

Substituting the rate equations provides

$$k_3^{(n)}\theta_{n-1}\theta_w - k_4^{(n)}\theta_n - k_5^{(n)}\theta_n = 0. \tag{36}$$

Rearranging and solving for the surface coverage of n solvated proton clusters gives

$$\theta_n = \theta_w \frac{k_3^{(n)}\theta_{n-1}}{k_4^{(n)} + k_5^{(n)}} \tag{37}$$

Now substituting Equation 32 into Equation 37 gives

$$\theta_n = \frac{NS + (n+\frac{1}{2})\theta_n k_4^{(n)}}{k_2 + (n+\frac{1}{2})\theta_{n-1}k_3^{(n)}} \times \frac{k_3^{(n)}\theta_{n-1}}{k_4^{(n)} + k_5^{(n)}} \tag{38}$$

Again, solving for the surface coverage of n solvated proton clusters and rearranging gives the explicit result,

$$\theta_n = \frac{N \cdot S}{k_5^{(n)}}\left(\frac{k_2^{(n)}k_4^{(n)}}{k_3^{(n)}k_5^{(n)}\theta_{n-1}} + \frac{k_2^{(n)}}{k_3^{(n)}\theta_{n-1}} + n + \frac{1}{2}\right)^{-1}. \tag{39}$$

Substituting this equation into the rate equation for ion emission (Eq. 24) and dividing through by the water flux term yields a dimensionless ion emission rate

$$\frac{r_c^{(n)}}{N \cdot S} = \left(\frac{k_2^{(n)}k_4^{(n)}}{k_3^{(n)}k_5^{(n)}\theta_{n-1}} + \frac{k_2^{(n)}}{k_3^{(n)}\theta_{n-1}} + n + \frac{1}{2}\right)^{-1}. \tag{40}$$

Substituting in the equations for each rate constant and rearranging leads to

$$\frac{r_c^{(n)}}{NS} = \left[\frac{A_2}{A_3^{(n)}\theta_{n-1}}\left(\frac{A_4^{(n)}}{A_5^{(n)}}e^{-(\lambda_v + \lambda_E^{(n)} - E_{Emit}^{(n)}(F))/kT} + e^{-(\lambda_v - E_A^{(n)})/kT}\right) + n + \frac{1}{2}\right]^{-1}. \tag{41}$$

For fields where ion emission is facile for a given cluster n, $E_{Emit}^{(n)} << \lambda_v + \lambda_E^{(n)}$. If it were not, signal from the n-1 cluster would also be observed. Additionally $A_4^{(n)} >> A_5^{(n)}$, since the time-scale for oscillation of one water molecule in a cluster is much smaller than the time-scale for an escape attempt of several molecules in concert. As a result, the first exponential term dominates the second, allowing us to neglect the latter. The sum $\lambda_v + \lambda_E^{(n)}$ is the vaporization energy plus the excess solvation energy which is the negative of the overall solvation energy for the n^{th} water molecule, $E_{Solv}^{(n)}$ from Equation 12. If we define

$$\kappa^{(n)} = \frac{A_2 A_4^{(n)}}{A_3^{(n)} A_5^{(n)} \theta_{n-1}}, \tag{42}$$

these assumptions allow us to simplify Equation 41 to provide

$$\frac{r_c^{(n)}}{N \cdot S} \cong \frac{1}{\kappa^{(n)} e^{-\left(\lambda_v + \lambda_E^{(n)}\right)/kT} + n + \frac{1}{2}}. \tag{43}$$

Equation 43 provides the functional form of the $H^+(H_2O)_n$ ion cluster emission rate equation for a constant optimal field. It contains a thermally activated reaction with an activation barrier equal to the solvation energy provided by the n^{th} solvating water molecule in the denominator. An equation describing the actual experimental ion signal illustrated in Figure 4 would require multiplication of the right hand side by a field dependent instrumentation constant. At low temperatures (while remaining above the condensation point) the ion emission rate is maximized and constant with

$$\frac{r_c^{(n)}}{N \cdot S} \cong \frac{1}{n + \frac{1}{2}} \qquad \lim T \rightarrow 0. \tag{44}$$

This predicts the plateaus observed in Figure 4, although absolute calibration of the ion signal is very difficult due to variations in ion collection efficiency with counter electrode

potential. As the temperature increases, the exponential term begins to dominate the denominator, and the ion signal decays according to

$$\frac{r_c^{(n)}}{N \cdot S} \cong \frac{1}{\kappa^{(n)}} e^{\left(\lambda_v + \lambda_E^{(n)}\right)/kT} \qquad \lim T \rightarrow \infty. \tag{45}$$

This form explains the unusual thermal deactivation of the ion emission event as well as the slope of the decay being equal to the solvation energy. The energy term in the exponential in Equation 45, $\lambda_v + \lambda_E^{(n)}$, corresponds to the energy required for removing the n^{th} solvating water molecule from the surface adsorbed protonated water cluster, to the surface, and then into the vacuum. This is equivalent to the total solvation energy provided to the surface adsorbed protonated water cluster by the n^{th} solvating water molecule, which are given in Table 1.

Conclusions

Water ion cluster $\{H^+(H_2O)_n\}$ formation and emission from a field adsorbed water layer on a Pt emitter tip was characterized for temperatures ranging from 170 K to 300 K. Mass resolved ramped field ionization experiments revealed a field dependence of ion cluster emission that varied with cluster mass. Large clusters were observed at lower field strengths. As the field increases, the cluster size decreases to successively lower values. This behavior is attributed to the tradeoff between the energetic favorabilty of large n cluster emission and the kinetic favorability of small n cluster emission. A comparison of the ion signals at different temperatures showed that the field required for emission of a specific cluster varied little with temperature, while the ion signal decayed with temperature. Constant field temperature cycling experiments provided Arrhenius plots showing thermal deactivation of ion emission for cluster sizes of n = 3, 4 and 5 with energies of 0.85, 0.76 and 0.55 eV, respectively. An analysis of the possible pathways available to an adsorbed ion cluster explains these thermal deactivation

energies as those associated with the solvation of the surface adsorbed proton by the n^{th} water molecule.

References

1 L. Onsager, Chemical Reviews **13**, 73 (1933).

2 D. Price and J. W. Halley, Journal of Electroanalytical Chemistry **159**, 347 (1983).

3 J. Kreuzer, Surface Science **246**, 336 (1991).

4 W. Schmickler, Surface Science **335** (1-3), 416 (1995).

5 M. G. Inghram and R. Gomer, Z. Naturforschg. **10a**, 863 (1955).

6 H. D. Beckey, *Principles of Field Ionization and Field Desorption Mass Spectrometry.* (Pergamon Press, Oxford, 1977).

7 W. A. Schmidt, Z. Naturforschg **19a**, 318 (1964).

8 A. R. Anway, The Journal of Chemical Physics **50** (5), 2012 (1969).

9 A. Stintz and J. A. Panitz, Journal of Applied Physics **72** (2), 741 (1992).

10 A. Stintz and J. A. Panitz, Surface Science **296** (1), 75 (1993).

11 A. Stintz and J. A. Panitz, International Journal of Mass Spectrometry and Ion Processes **133** (1), 59 (1994).

12 D. L. Scovell, T. D. Pinkerton, B. A. Finlayson, and E. M. Stuve, Submitted to Chemical Physics Letters (1998).

13 D. L. Scovell, T. D. Pinkerton, V. K. Medvedev, and E. M. Stuve, Proceedings of the Electrochemical Society **5**, 6 (1999).

14 D. L. Scovell, T. D. Pinkteron, V. K. Medvedev, and E. M. Stuve, Surface Science **457** (3), 365 (2000).

15 T. D. Pinkerton, D. L. Scovell, A. L. Johnson, B. Xia, V. Medvedev, and E. M. Stuve, Langmuir **15** (3), 851 (1999).

16 P. L. Geissler, C. Dellago, D. Chandler, J. Hutter, and M. Parrinello, Science **291** (16 March), 2121 (2001).

17 L. A. Montero, J. Molina, and J. Fabian, International Journal of Quantum Chemistry **79** (1), 8 (2000).

18 J. A. Mejias and S. Lago, Journal of Chemical Physics **113** (17), 7306 (2000).

19 M. F. Kropman and H. J. Bakker, Science **291** (16 March), 2118 (2001).

20 E. R. Batista, S. S. Xantheas, and H. Johnnson, Journal of Chemical Physics **112** (7), 3285 (2000).

21 G. F. Rempfer, Journal of Applied Physics **57** (7), 385 (1985).

22 M. q. Kato and T. Katsushige, Nuclear Instruments and Methods in Physics Research A **298**, 296 (1990).

23 R. Gomer, *Field emission and field ionization.* (Harvard University Press, Cambridge, 1961).

24 T. T. Tsong, *Atom-probe field ion microscopy - Field ion emission and surface and interfaces at atomic resolution.* (Cambridge University Press, Cambridge, 1990).

25 *Handbook of chemistry and physics,* edited by D. R. Lide (CRC Press, Boca Raton, 1995).

26 D. Eisenberg and W. Kauzmann, *The structures and properties of water.* (Oxford University Press, New York and Oxford, 1969).

27 D. W. Smith, Journal of Chemical Education **54** (9), 540 (1977).

28 M. Meot-Ner, Journal of the American Chemical Society **108** (20), 6189 (1986).

29 J. Jeans, *The Mathematical Theory of Electricity and Magnetism.* (University Press, Cambridge, 1966).

30 V. K. Medvedev, N. N. Popovich, and A. O. Snitko, Soviet Physics, Technical Physics **36** (2), 223 (1991).

31 C. J. Rothfuss, V. K. Medvedev, and E. M. Stuve, Unpublished (2001).

32 N. Ernst, G. Bozdech, V. Gorodetskii, H. J. Kreuzer, R. L. C. Wang, and J. H. Block, Surface Science **318** (3) (1994).

LIST OF FIGURE CAPTIONS

Figure 1

Wien filter and lens apparatus. I. System schematic showing flight path of ions for masses m_0 and m: (a) tip at potential V_t and counter electrode at potential V_{CE}, (b) lens assembly at potential V_L, (c) ExB Wien filter, (d) bellows, (e) drift tube, (f) ion detector comprised of dual chevron multi-channel plates and a phosphor screen, (g) CCD camera for imaging and focusing ion signal. II. Design of lens assembly: (b_1) entrance diaphragm, (b_2) front electrode, (b_3) center electrode, (b_4) back electrode. III. Cross sectional diagram of ExB Wien filter: (c_1) magnet, (c_2) electrode support, (c_3) electrode, (c_4) lens support rods.

Figure 2

Mass selected ramped field cluster formation. (a) Protonated water clusters, $H^+(H_2O)_n$, with n up to 7 were observed while ramping the applied field on a Pt emitter tip (~350Å) from 0 to 1.6 V/Å. The experimental background H_2O partial pressure was 5 10^{-6} Torr. (b) A magnification of the high mass cluster signal for the 180K ramped field experiments.

Figure 3

Typical ion cluster formation dependency during temperature cycling (lower curves). The tip potential was held at the optimal formation potential (see Fig. 2) for each respective ion while the temperature of the tip was slowly cycled linearly with time (upper curves).

Figure 4

Arrhenius plot of cluster ion formation during temperature cycling demonstrating thermal *deactivation* of the cluster emission. Deactivation energies determined from the slopes of the solid lines are 0.85 ± 0.03 eV, 0.76 ± 0.02 eV and 0.55 ± 0.02 eV for n = 3, 4 and 5, respectively.

Figure 5

Field bending of potential energy barriers to ion cluster emission. The energies for emission of clusters *n* = 1-4 under field free conditions are shown by the short dashed lines. Image potential and field lines are illustrated with thin solid and long dashed lines, respectively. Energies are referenced to uncharged water adsorbed on the platinum tip surface. The resulting emission barriers confronted by the solvated proton on the surface are shown by the thick solid curves. As the field increases, the barriers in turn fall below the energy of the solvated proton on the surface.

Figure 6

(a) Possible reaction pathways for an adsorbed water cluster. The cluster may be solvated by additional water molecules (if available) desorb from the surface, or lose a solvating water molecule. (b) Reaction barrier energy diagram for solvation. $\lambda_E^{(n)}$ represents the excess solvation energy of the n^{th} solvating water molecule.

LIST OF TABLE CAPTIONS

Table 1

Ion cluster energies and observed formation fields.

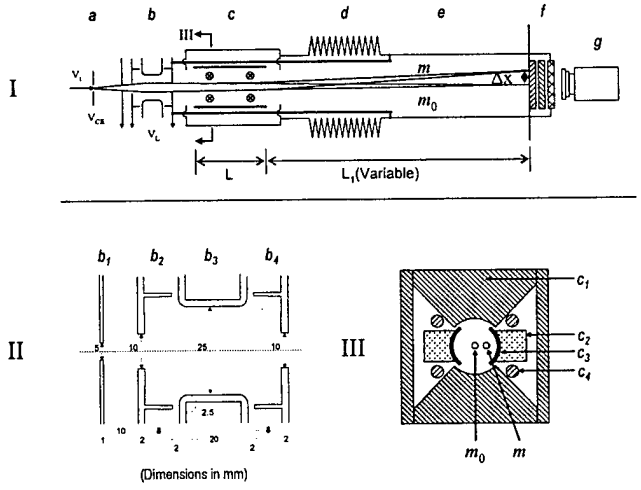

FIGURE 1

C. J. Rothfuss
J. Chem. Phys.

(a)

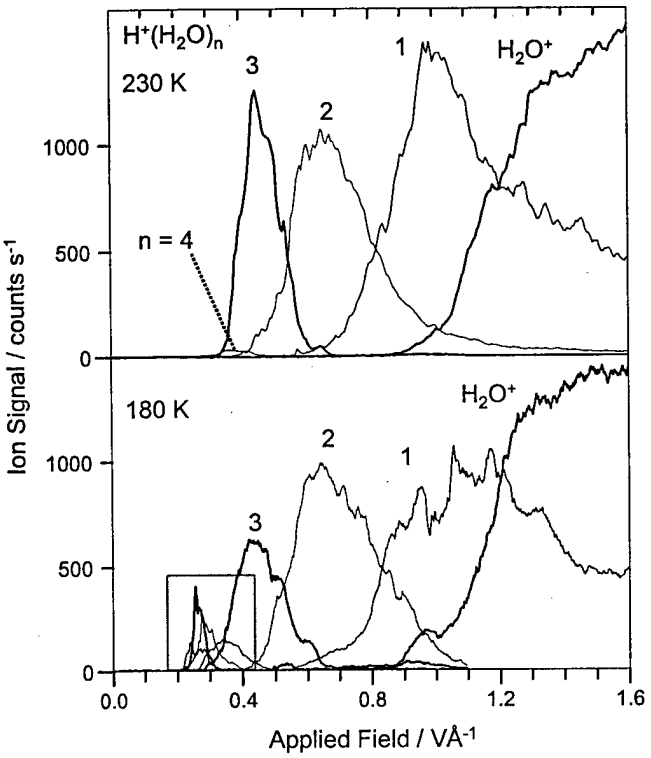

(b)

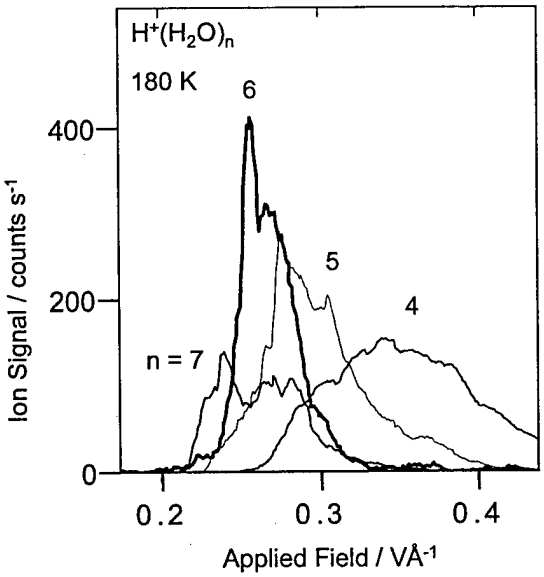

FIGURE 2

C. J. Rothfuss
J. Chem. Phys.

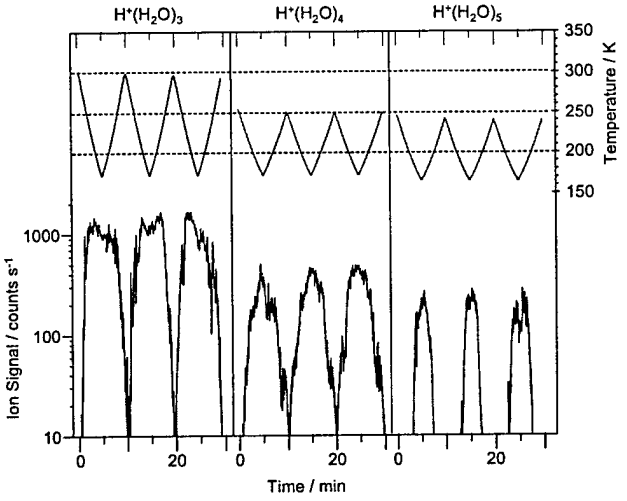

FIGURE 3

C. J. Rothfuss
J. Chem. Phys.

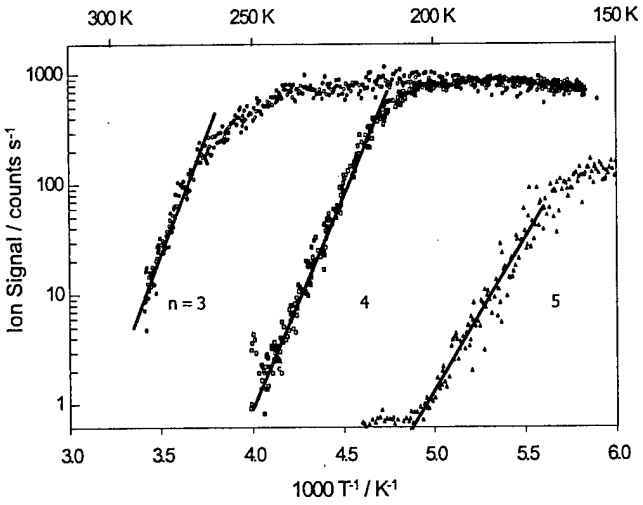

FIGURE 4

C. J. Rothfuss
J. Chem. Phys.

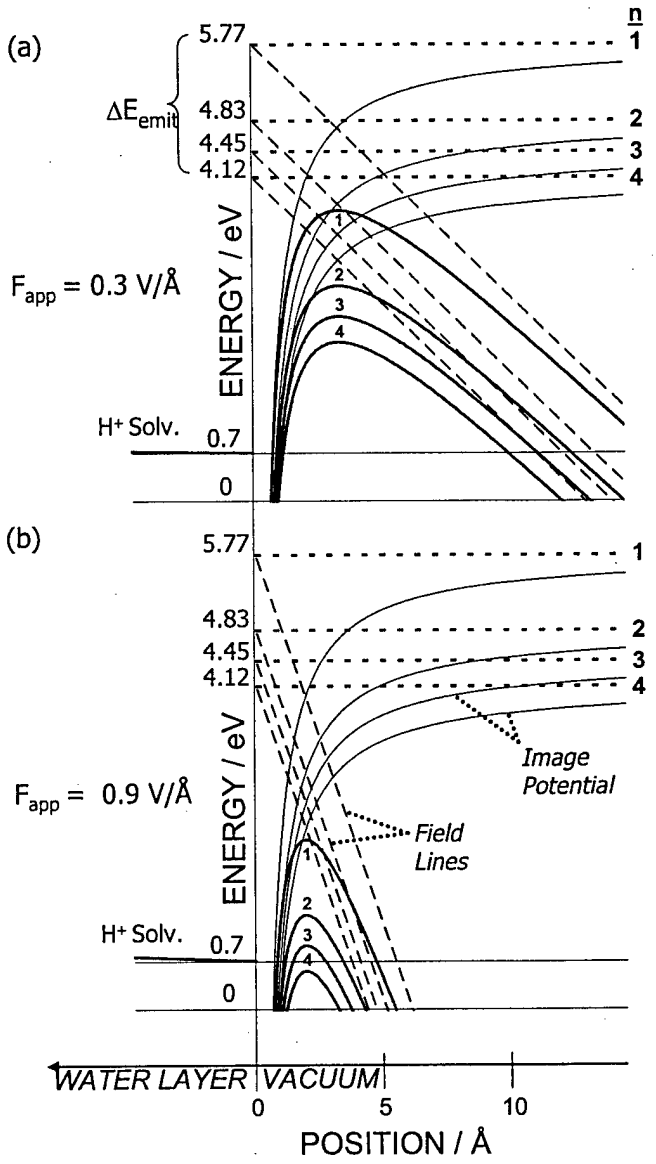

FIGURE 5

C. J. Rothfuss
J. Chem. Phys.

(a)

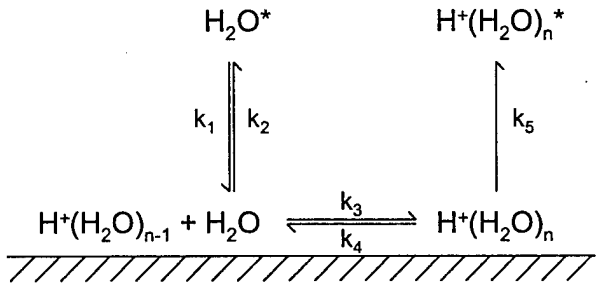

(b)

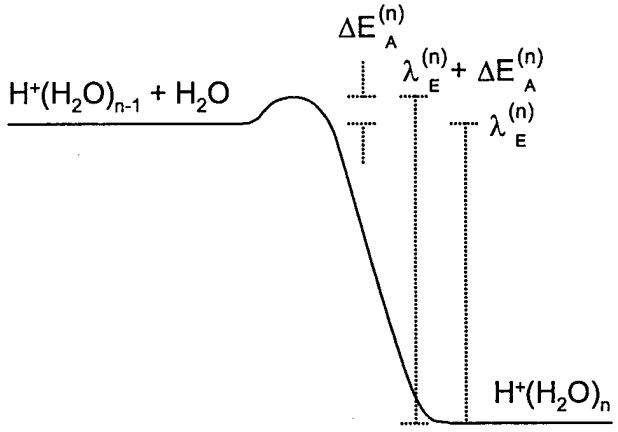

FIGURE 6

C. J. Rothfuss
J. Chem. Phys.

	F_{app} [a] V/Å	Lit ΔE_{solv} [b] eV	Exp ΔE_{solv} [c] eV	ΔE_{emit} [d] eV
H^+	n/a	n/a	-	12.55
$H^+(H_2O)$	1.00	-7.22	-	5.77
$H^+(H_2O)_2$	0.64	-1.38	-	4.83
$H^+(H_2O)_3$	0.45	-0.82	-0.85	4.45
$H^+(H_2O)_4$	0.34	-0.76	-0.76	4.12
$H^+(H_2O)_5$	0.29	-0.50	-0.55	4.07
$H^+(H_2O)_6$	0.27	-0.48	-	4.02
$H^+(H_2O)_7$	0.26	-0.46	-	4.00

[a] Optimal observed applied field for cluster formation.

[b] H^+ solvation energy associated with *n*-1 to *n* transition. [Meot-Ner]

[c] Experimentally observed solvation energies.

[d] Calculated emission energy based on $\Delta E_{solv}+\lambda_v$ (e.g. $\Delta E_{emit}(n=3)$ = 4.83 eV - 0.82 eV + 0.44 eV = 4.45 eV)

TABLE 1

C. J. Rothfuss
J. Chem. Phys.